

**SYNTHESIS, CHARACTERIZATION AND EVALUATION OF  
POLYMER-IRON OXIDE HYBRID NANOSYSTEMS FOR  
TARGETING AND IMAGING APPLICATIONS**

**SHVETA MAHAJAN**



**CENTRE FOR POLYMER SCIENCE AND ENGINEERING  
INDIAN INSTITUTE OF TECHNOLOGY DELHI  
AUGUST 2012**

© Indian Institute of Technology Delhi (IITD), New Delhi, 2012

**SYNTHESIS, CHARACTERIZATION AND EVALUATION OF  
POLYMER-IRON OXIDE HYBRID NANOSYSTEMS FOR  
TARGETING AND IMAGING APPLICATIONS**

*by*

**SHVETA MAHAJAN**

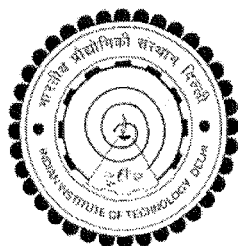
**Centre for Polymer Science and Engineering**

**Submitted**

*In fulfillment of the requirements of the degree of*

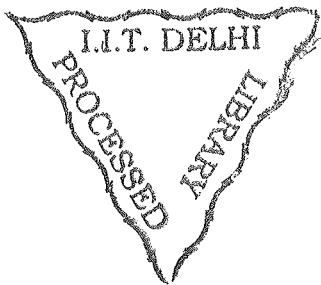
**Doctor of Philosophy**

*to the*



**Indian Institute of Technology Delhi  
August 2012**

I.I.T. DELHI.  
LIBRARY  
Acc. No. TH8544.....



TH  
620.3:616-073  
MAH-S

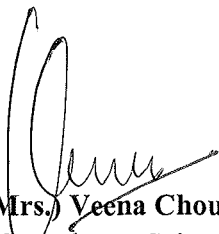
Dedicated to my Parents



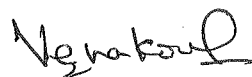
## CERTIFICATE

This is to certify that the thesis entitled “**Synthesis, Characterization and Evaluation of Polymer-Iron Oxide Hybrid Nanosystems for Targeting and Imaging Applications**” being submitted by **Ms. Shveta Mahajan** to the Indian Institute of Technology, Delhi for the award of the degree of **Doctor of Philosophy** is a record of bona fide research work carried out under our guidance and supervision and has fulfilled the requirements for the submission of this thesis, which to our knowledge has reached the requisite standard.

The results contained in this thesis are original and have not been submitted, in part or in full, to any other University or Institute for the award of any other degree or diploma.



**Prof. (Mrs.) Veena Choudhary**  
Centre for Polymer Science and Engineering  
Indian Institute of Technology Delhi  
Hauz Khas, New Delhi-110016



**Prof. (Mrs.) Veena Koul**  
Centre for Biomedical Engineering  
Indian Institute of Technology Delhi  
Hauz Khas, New Delhi-110016



## ACKNOWLEDGEMENTS

My sincere thanks to the many people who made this work possible-

I express gratitude to my supervisors Prof. Veena Choudhary and Dr. Veena Koul for their guidance, which has been a constant source of inspiration. Their suggestions and advice have been invaluable and working with them has been a truly enriching experience.

I express my sincere thanks to Prof. S. N. Maiti, Prof. A.K. Ghosh, Prof. Harpal Singh, Dr. Josemon Jacob and Dr. Bhabani Satapathy for their encouragement and help throughout my work.

I gratefully acknowledge the Council for Scientific and Industrial Research, India for Junior and Senior Research Fellowships received, and the Department of Science and Technology (DST), India and École Polytechnique Fédérale de Lausanne (EPFL), Switzerland for the chance to work at the University of Fribourg under the Indo-Swiss Joint Research Programme. I owe my thanks to Prof. Alke Fink for the opportunity to work with her at the Department of Chemistry, University of Fribourg, and making available the support and lab facilities there. The time spent with her group will always be an invaluable and memorable part of my life.

I also express my gratitude to Dr. Amit K. Dinda, Department of Pathology, AIIMS, Delhi and Dr. Alok C. Bharati, Division of Molecular Oncology, Institute for Cytology and Preventive Oncology (ICPO), Noida, for allowing me to work in their laboratories. I am grateful to Dr. R. K. Kotnala at the Dept. of Materials Physics and Engineering, National Physical Laboratory (NPL), Delhi, who permitted me to conduct magnetic property measurements in his laboratory.

My special thanks to Mr. Surender Sharma, Mrs. Rama and Mr. Shivkant from CPSE, IIT Delhi who were always kind and helpful.

I owe my gratitude to Mr. Anil Pandey, Biosensor Laboratory, CBME, IIT Delhi, for help in animal handling and to Mr. Pradeep in the laboratory at Renal Pathology Laboratory, AIIMS, Delhi. I am grateful to Mr. Khanna, Mr. Munna Lal and Dr. Deepak Varandani at IIT Delhi who helped with TEM, NMR and AFM acquisitions respectively. Dr. Gajendra

Saini at the Jawaharlal Nehru University, Delhi was an immense help with HRTEM studies.

I acknowledge my colleagues, seniors and contemporaries at CPSE - Dipti, Pooja, Neetu, Pravin, Geeta, Piyush, Anju, Deeksha, Rajender and Sandeep for their friendship and cooperation. I thank my labmates Rachna, Nany, Shantanu, Arun, Alex, and Manisha at CBME, IIT Delhi for their help. I am grateful to Prashant and Farhat from AIIMS and Gauri at ICPO for their help in cell culture experiments. I appreciate the cooperation and help of Jyoti at NPL with magnetization studies. Thanks also to my colleagues at Fribourg – Nok, Isabelle, Andrea, Cecil, Anthony, Reinaldo, Vera and Calum – it was good knowing you all.

A big heartfelt ‘thank you’ to my friends Preeti, Sneha, Anshul, Shrutika and Gayathri for being an incredible support system all through my PhD – I am so lucky.

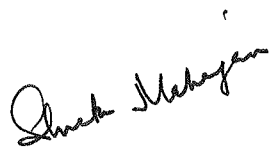
I have to express my deepest regards and affection for Massiji and her family. For six years Maya Enclave has been a home away from home. Peush Chacha and Deepa Chachi, and Rajneesh Chacha and Meenakshi Chachi have been very caring all this time. My cousins are always great for a laugh and a conversation. It has been good.

To my parents I will always be indebted for their unquestioning love, support, and patience. I am humbled by and grateful for their faith in me. I thank my family, my brother Mohit, my sister-in-law Sitanshi for their caring and affection, and the babies Kartik and Deetya, who light up my life.

And then, Mohit – thank you for being there.

Thanks to all other family and friends, who listened, motivated and believed.

Lastly, importantly – with humility and gratitude I thank God for helping me accomplish this undertaking.



**Shveta Mahajan**

## ABSTRACT

The use of nanoparticles in nanomedicine offers various exciting possibilities. In recent years, nanoparticles have revolutionised the approach to the systemic delivery of pharmaceutically active compounds; they provide controlled release, eliminate side-effects and maximise the therapeutic efficacy of a drug. In the case of nanoparticles used for diagnostics and imaging, the active agent may be directed to the particular cells, tissues or organs of interest by use of targeting moieties that 'home in' on the specific region.

One of the most promising candidates in medical diagnostics are the iron oxide nanoparticles, which below a certain critical value (typically in the 5-20 nm range) exhibit superparamagnetism. This thesis deals with the development of systems based on superparamagnetic iron oxide nanoparticles (SPIONs) for contrast enhancement in magnetic resonance imaging (MRI). The thesis is divided into four parts. The first part describes the synthesis and characterization of SPIONs prepared by two alternative thermal decomposition methods. The second part deals with the encapsulation of SPIONs in a micellar system and their conjugation with folic acid. The SPION-micelle systems were characterized and evaluated for receptor-mediated internalization in HeLa cells, besides magnetic targeting ability to a tumor in an *in vivo* model. The third part deals with the stabilization of SPIONs with a gelatin coating, mannosylation and the evaluation of this system for mannose receptor targeting efficacy. The fourth part describes the PEGylation of the surface of hydrophobic SPIONs, to facilitate their transfer to aqueous medium.

The first experimental chapter in this thesis describes in detail two synthetic routes for the preparation of highly crystalline SPIONs, by decomposition of iron organic precursors in organic

solvents. The first route involved decomposition of iron (III) acetylacetonate in triethylene glycol (TREG) and resulted in hydrophilic TREG-coated SPIONs [SPIO(L)]. SPIONs prepared by varying reaction conditions had particle size  $4.95 \pm 1.12$  nm [SPIO<sub>0.5</sub>(L)] and  $9.27 \pm 3.37$  nm [SPIO<sub>1</sub>(L)]. These nanoparticles were characterized by TEM, XRD, FTIR, TGA and VSM. The larger particles, designated as SPIO<sub>1</sub>(L), possessed a high magnetization value of 76.8 emu/g of iron oxide (IO), while SPIO<sub>0.5</sub>(L) had a magnetization of 55.6 emu/g of iron oxide (IO).

The second method adopted for SPION synthesis involved the thermal decomposition of iron (III) oleate in 1-octadecene in the presence of oleic acid and produced highly hydrophobic oleic acid-coated SPIONs [SPIO(B)]. These SPIONs had a small size and were highly monodisperse (diameter =  $5.24 \text{ nm} \pm 0.30 \text{ nm}$ ). They were characterized by TEM, FTIR, TGA and VSM. These too possessed a high value of magnetization (73.6 emu/g of IO).

Chapter 3 describes the preparation of SPION-polymeric hybrid micelles from SPIO<sub>1</sub>(L) and a PMMA-b-pPEGMA copolymer conjugated with folic acid, for a dual targeting ability, i.e. via the folate receptor (FR) for receptor-mediated internalization and by magnetic targeting with the aid of an external magnetic field. The PMMA-b-pPEGMA copolymers were first prepared by atom transfer radical polymerization (ATRP) and characterized by GPC and <sup>1</sup>H-NMR. The polymer designated as M<sub>1</sub>EG<sub>1</sub> was conjugated with folic acid (the folate-conjugated polymer is designated as FM<sub>1</sub>EG<sub>1</sub>). Critical micellar concentrations (CMC) were determined for all the polymers and it was found that with the length of the hydrophobic core (PMMA) remaining the same, the length of the hydrophilic block did not show any significant effect on CMC, while an increase in the length of the hydrophobic block or conjugation with folic acid led to a drastic lowering of CMC. Micelles prepared from M<sub>1</sub>EG<sub>1</sub> and FM<sub>1</sub>EG<sub>1</sub> were characterized by TEM,

AFM and DLS. Micelles made from M<sub>1</sub>EG<sub>1</sub> had a hydrodynamic radius of 95.82 nm (PDI=0.073), while FM<sub>1</sub>EG<sub>1</sub> micelles had a diameter 118.7 nm (PDI 0.108). A core-shell morphology was discernible in the TEM micrographs of the micelles. These micelles were used to prepare SPION-polymer hybrids by aqueous desolvation of a mutual solution of the SPIONs and polymer in tetrahydrofuran. The SPION-polymer micelles were characterized by TEM and MRI. T<sub>2</sub> relaxivity was determined for SPIO<sub>1</sub>(L)- FM<sub>1</sub>EG<sub>1</sub> micelle cluster and was found to be 260.4 mM<sup>-1</sup>sec<sup>-1</sup>. *In vitro* cytotoxicity and uptake was evaluated in HeLa cells. The cells showed nearly 90% viability when treated with SPIONs at a concentration of 20 µg/ml (Fe) for 24 h. Internalization studies (Prussian blue quantification and confocal microscopy of Nile red loaded micelles) revealed that the folate-conjugated SPION-micelles were internalized more efficiently by the HeLa cells, which overexpress the folate-receptor, than the unconjugated formulation.

In chapter 4 the encapsulation of TREG-coated SPION in a stabilizing gelatin coat is discussed. The SPION-loaded nanoparticles were further mannosylated for mannose receptor-mediated targeting of macrophages. First the method for preparing gelatin nanoparticles (GNP) (desolvation) was optimized for pH, gelatin and crosslinker (glutaraldehyde) concentration. Particles having ~110 nm diameter could be produced and were characterized by TEM, AFM and DLS. TREG-coated SPIONs were then incubated with gelatin, the dispersion subjected to desolvation under the appropriate pH and concentration conditions and crosslinked with glutaraldehyde. The SPION-loaded gelatin nanoparticles were then derivatized with mannose. Non-mannosylated and mannosylated nanoparticles were referred to as MGNP and MN-MGNP respectively. Characterization was done by DLS, TEM and FTIR. MGNP had a hydrodynamic diameter of 163.3 nm (PDI = 0.113), while MN-MGNP exhibited an increased size of 221.4 nm (PDI = 0.095). Colloidal stability was established in water, PBS (pH 7.4), electrolyte solution

(1M NaCl), cell culture medium (DMEM) with and without serum and it was found that both MGNP and MN-MGNP were stable/non-aggregating in these media. The stability of nanoparticles in PBS over a period of several days was also established by measuring hydrodynamic diameter of MGNP and MN-MGNP in dispersions stored at 4 °C.

T2 relaxivities were also determined for MGNP and MN-MGNP by *in vitro* MR imaging, and were found to be 168.7 and 158.2 mM<sup>-1</sup>sec<sup>-1</sup> respectively, which is comparable to commercially available agents.

Cell studies were done using the J774e murine macrophage cell line. These cells upregulate the mannose receptor. A cell viability of 92.99±2.67% and 91.13±3.35% was determined for MGNP and MN-MGNP respectively after an incubation period of 24 h at a concentration of 20 µg/ml. Cellular internalization was studied by quantifying iron oxide internalized in J774e cells by colorimetric Prussian blue assay. MN-MGNP were internalized to a greater extent in these cells than the MGNP.

The final experimental chapter described the modification of oleic acid-coated SPIONs with PEG-silanes synthesized in the laboratory. Copolymers of poly(ethylene glycol) methyl ether methacrylate (PEGME-MA, Mn=300) and 3-(trimethoxysilyl)propyl methacrylate (TMSPMA) were prepared by free-radical polymerization and characterized by GPC and FTIR. Carboxy functionality was introduced by using trimethylsilyl methacrylate (TMSMA) as one of the monomers with eventual deprotection of the trimethylsilyl groups which protect carboxy functionality. SPIONs modified with a neutral PEG silane were designated as MNP-Si-PEG, while those modified with TMSMA-containing polymers were called MNP-Si-CPEG1 and MNP-Si-CPEG2 (after deprotection of the carboxy groups). MNP-Si-CPEG2 had a greater

TMSMA content in the original polymer than MNP-Si-CPEG1. MNP-Si-CPEG1 and MNP-Si-CPEG2 were then conjugated with PEI ( $M_n=600$ ) subsequently, with the PEI modified SPIONs designated as MNP-PEI1 and MNP-PEI2 respectively. The modified SPIONs were characterized by TEM, DLS, FTIR and TGA. All possessed hydrodynamic diameters of less than 10 nm. Their colloidal stability was established in different media including water, PBS, 1 M NaCl and cell culture medium (RPMI) with and without serum by measuring their UV absorption. T2 relaxivity of the sample MNP-Si-PEG was determined to be  $114.8 \text{ mM}^{-1}\text{sec}^{-1}$ .

*In vitro* studies included MTT assay and quantification of cellular uptake of the particles and were done with HeLa cells. MNP-Si-PEG, MNP-Si-CPEG1 and MNP-Si-CPEG2 were non-toxic to the cells treated for 24 h. MNP-PEI1 and MNP-PEI2 however, caused a lowering in the cell viability for the same period of incubation. Cell uptake studies by Prussian blue assay revealed that for MNP-Si-PEG and MNP-Si-CPEGs 1 and 2, SPION internalization increased as the time of incubation was increased from 1 to 24 h. With the PEI-conjugated SPIONs, cell uptake was greater after 6 h of incubation as compared to 1 h. This was, however, followed by a saturation of particle concentration within the cells.

Thus, this work demonstrates that SPIONs produced by different strategies offer versatility with respect to polymeric modification depending upon the application envisaged. The variously modified SPIONs showed good biocompatibility and cellular internalization kinetics and have potential for application as MRI contrast agents.



## TABLE OF CONTENTS

ACKNOWLEDGEMENTS.....	i
ABSTRACT.....	iii
TABLE OF CONTENTS.....	viii
LIST OF FIGURES.....	xv
LIST OF TABLES.....	xix
ABBREVIATIONS.....	xx
<b>CHAPTER I - Introduction and Literature Review.....</b>	<b>1</b>
1.1. Nanotechnology.....	1
1.2. Nanomedicine.....	2
1.2.1. Types of Nanocarriers.....	4
1.3. Targeting Strategies.....	6
1.3.1. Passive Targeting.....	6
1.3.2. Active Targeting.....	8
1.3.2.1. Mannose Receptor.....	8
1.3.2.2. Folate Receptor.....	10
1.4. Magnetic Resonance Imaging (MRI) .....	12
1.4.1. T1 Relaxation.....	13
1.4.2. T2 Relaxation.....	14
1.4.3. T2* (T2 Star) .....	15
1.4.4. Contrast Agents.....	15
1.4.4.1. Positive Contrast Agents.....	15
1.4.4.2. Negative Contrast Agents.....	16
a. Superparamagnetic Iron Oxide (SPIO).....	16
b. Ultrasmall Superparamagnetic Iron Oxide (USPIO).....	17

1.4.5. Superparamagnetic Iron Oxide Nanoparticles for Magnetic Resonance Imaging.....	19
1.4.5.1. Composition and Structure.....	19
1.4.5.2. Magnetic behavior of iron oxides.....	20
1.4.5.3. Methods of Synthesis.....	22
1.4.5.4. Stabilization.....	25
1.5. Scope of the Present Work.....	26
1.6. Objective.....	26
1.7. Format of the Thesis.....	28
References.....	30

**CHAPTER II - Synthesis and Characterization of Superparamagnetic Iron Oxide Nanoparticles (SPIONs) .....39**

2.1. Introduction.....	39
2.2. Synthesis and Characterization of Hydrophilic Iron Oxide Nanoparticles.....	39
2.2.1. Experimental.....	39
2.2.1.1. Materials.....	39
2.2.1.2. Synthesis of SPIONs.....	39
2.2.2. Characterization.....	40
2.2.2.1 Morphological Characterization.....	40
2.2.2.2. X-Ray Diffraction (XRD) .....	41
2.2.2.3. Thermogravimetric Analysis (TGA) .....	41
2.2.2.4 Fourier Transform- Infrared Spectroscopy (FT-IR) .....	41
2.2.2.5. Magnetization.....	41
2.2.3. Results and Discussion.....	41
2.2.3.1. Microstructure.....	42
2.2.3.2. Surface Coating- Characterization by TGA, FT-IR.....	44
2.2.3.3. Magnetization.....	45
2.3. Synthesis and Characterization of Hydrophobic Iron Oxide Nanoparticles.....	47
2.3.1 Experimental.....	47

2.3.1.1. Materials.....	47
2.3.1.2. Synthesis of SPIONs.....	47
2.3.2. Characterization.....	49
2.3.3. Results and Discussion.....	49
2.4. Conclusion.....	53
References.....	55

**CHAPTER III - Preparation of SPION-Polymer Micelles and their Evaluation for Folate Receptor Targeting.....56**

3.1. Introduction.....	56
3.2. Experimental.....	57
3.2.1. Materials.....	57
3.2.2. Methods.....	58
3.2.2.1 Preparation of PMMA-b-pPEGMA Copolymers.....	58
3.2.2.2. Folate Conjugation.....	59
3.2.2.3. Preparation of Polymeric Micelles.....	59
3.2.2.4. SPION-Micelle Clusters.....	60
3.3. Characterization.....	61
3.3.1. Gel Permeation Chromatography (GPC) .....	61
3.3.2. NMR Spectroscopy.....	61
3.3.3. UV-Vis Spectroscopy.....	61
3.3.4. Morphological Characterization.....	61
3.3.5. Critical Micellar Concentration (CMC) .....	62
3.3.6. Magnetization .....	62
3.3.7. Magnetic Resonance Imaging (MRI) .....	63
3.3.8. Biological Evaluation- In Vitro Studies.....	63
3.3.8.1. Cellular Toxicity.....	63
3.3.8.2. Cellular Internalization- Quantification by Prussian Blue Method.....	64
3.3.8.3. Cellular Internalization- Confocal Microscopy.....	64

3.3.9. Statistical Analysis.....	65
3.4. Results and Discussion.....	65
3.4.1. Polymer Synthesis.....	65
3.4.2. Folate Conjugation of PMMA-pPEGMA Block Copolymer.....	68
3.4.3. Micellization.....	69
3.4.4. Magnetic Resonance Imaging.....	73
3.4.5. Biological Evaluation.....	76
3.4.5.1. Cellular Toxicity.....	76
3.4.5.1. Cellular Internalization.....	77
3.5. Conclusion.....	81
References.....	82

**CHAPTER IV - Development of Mannose-Conjugated Gelatin Nanoparticles for Macrophage Targeting.....84**

4.1. Introduction.....	84
4.2. Experimental.....	85
4.2.1. Materials.....	85
4.2.2. Methods.....	86
4.2.2.1. Optimization of Gelatin Nanoparticle (GNP) preparation.....	86
4.2.2.2. Preparation of SPION loaded GNP.....	86
4.2.2.3. Mannosylation of MGNP.....	87
4.3. Characterization.....	88
4.3.1. Morphological Characterization.....	88
4.3.2. Fourier Transform- Infrared Spectroscopy (FT-IR).....	89
4.3.3. Determination of Fe content.....	89
4.3.4. Colloidal Stability.....	89
4.3.5. Magnetic Resonance Imaging (MRI) .....	90
4.3.6. Biological evaluation.....	90
4.3.6.1. Cellular toxicity.....	90
4.3.6.2. Cellular Internalization- Quantification by Prussian Blue Method.....	91

4.3.6.3. Cellular Internalization- Inverted Light Microscopy.....	91
4.3.7. Statistical Analysis.....	92
4.4. Results and Discussion.....	92
4.4.1. Optimization of Nanoparticle (GNP) Preparation by Desolvation.....	92
4.4.2. Preparation of MGNP and Mannosylation- Morphological Characterization, Charge Determination and FT-IR.....	96
4.4.3. Colloidal Stability.....	98
4.4.4. Magnetic Resonance Imaging (MRI) .....	101
4.4.6. Biological Evaluation.....	102
4.4.6.1. Cellular toxicity (MTT Assay).....	102
4.4.6.2. Cellular Internalization- Quantification by Prussian Blue Method.....	104
4.4.6.3. Cellular Internalization- Inverted Light Microscopy.....	106
4.5. Conclusion.....	107
References.....	109

**CHAPTER V - Surface Modification of SPIONs - Characterization and *In Vitro* Studies.....110**

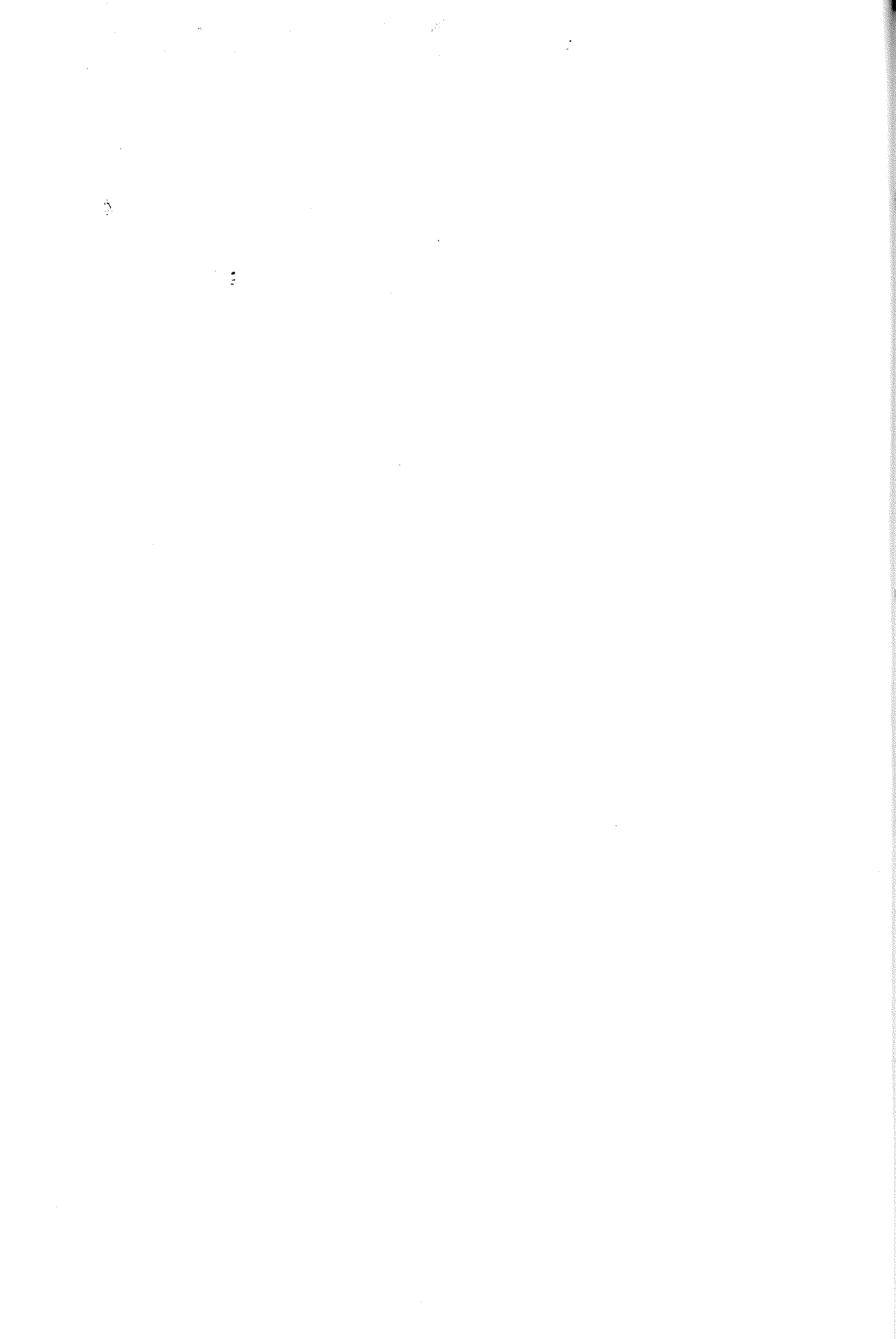
5.1. Introduction.....	110
5.2. Experimental.....	111
5.2.1. Materials.....	111
5.2.2. Synthesis of PEG-Silanes.....	111
(a) p(PEGME-MA-r-TMSPMA) [CP1] .....	111
(b) p(PEGME-MA-r-TMSMA-r-TMSPMA) [CP2 and CP3].....	112
5.2.3. Copolymer Characterization.....	114
5.2.4. SPION Surface Functionalization- Exchange of Oleic Acid with PEG-Silane.....	114
5.2.5. Transfer to Aqueous Medium (PBS, pH 7.4).....	115
5.2.6. Conjugation with PEI.....	116
5.2.7. Nanoparticle Characterization.....	116
5.2.8. Determination of Fe content.....	117

5.2.9. Colloidal Stability.....	117
5.2.10. Magnetic Resonance Imaging (MRI) .....	118
5.2.11 Cell Culture.....	118
5.2.12. Evaluation of Cell Viability.....	118
5.2.13. Particle Uptake.....	119
5.2.14. Statistical Analysis.....	119
5.3 Results and Discussion.....	119
5.3.1. Copolymer Composition.....	120
5.3.2. Ligand Exchange and Transfer to Water.....	122
5.3.3. FT-IR.....	125
5.3.4. Thermogravimetric Analysis.....	128
(a) MNP-Si-PEG.....	128
(b) MNP-Si-CPEG1 and MNP-Si-CPEG2.....	128
(c) MNP-PEI1 and MNP-PEI2.....	129
5.3.5. Colloidal Stability.....	130
5.3.6. Magnetic Resonance Imaging.....	132
5.3.7. Biological Evaluation.....	134
5.3.7.1. Cytotoxicity (MTT Assay) .....	134
5.3.7.2. In Vitro Uptake- Prussian Blue Assay.....	135
5.4. Conclusion.....	136
References.....	137
<b>CHAPTER VI - Summary, Conclusions and Future Perspectives.....</b>	<b>139</b>
6.1. Introduction.....	139
6.2. Synthesis and Characterization of Superparamagnetic Iron Oxide Nanoparticles (SPIONs).....	140
6.3. Preparation of SPION-Polymer Micelles and their Evaluation for Folate Receptor Targeting.....	142
6.4. Development of SPION-Loaded Gelatin Nanoparticles for Mannose Receptor Targeting.....	145

6.5. Surface Modification of SPIONs – Characterization and In Vitro  
Studies.....148

6.6. Conclusions.....151

6.7. Future Perspectives.....154



## LIST OF FIGURES

Figure no.	Figure title	Page no.
Figure 1.1	Types of nanocarriers for drug delivery/imaging applications.	6
Figure 1.2	Extravasation of particulate nanocarrier from circulation into the tumor microenvironment across hyperpermeable endothelium.	7
Figure 1.3	Representation of (a) macrophage phagocytosing a bacterium and (b) receptor-mediated internalization of a particulate drug-carrier.	10
Figure 1.4	Schematic representation of transmembrane transport of the folate receptor mediated by caveolae.	12
Figure 1.5	Magnetization M as a function of applied magnetic field H	22
Figure 1.6	A summary of published work available on iron oxide nanoparticle synthesis by physical, chemical and biological routes.	24
Figure 2.1	Synthesis of TREG-coated SPIONs– Thermal decomposition of Fe (III) acetylacetonate.	40
Figure 2.2	SPIO <sub>1</sub> (L) – (a) TEM micrograph (b) HRTEM of single crystallite showing lattice planes, (c) SAED, (d) XRD pattern; SPIO <sub>0.5</sub> (L)– (e) TEM micrograph, (f) SAED pattern.	44
Figure 2.3	TG scans of– (a) SPIO <sub>1</sub> (L) and (b) SPIO <sub>0.5</sub> (L) in N <sub>2</sub> atmosphere (heating rate 10 °C/min).	45
Figure 2.4	FT-IR spectrum– SPIO <sub>1</sub> (L).	45
Figure 2.5	M vs H curves– (a) SPIO <sub>1</sub> (L) and (b) SPIO <sub>0.5</sub> (L); insets show low field region.	46
Figure 2.6	SPION synthesis– (a) synthesis of ferric oleate, (b) thermal decomposition of iron (III) oleate to yield oleic acid-coated SPIONs.	48
Figure 2.7	(a) TEM micrograph of oleic-acid coated SPIONs dispersed in hexane and (b) histogram depicting particle size distribution of SPIONs.	49
Figure 2.8	FT-IR Spectra of (a) oleic acid, (b) Fe (III) oleate and (c) Oleic acid-coated SPIONs [SPIO(B)].	50
Figure 2.9	Modes of coordination of oleate with iron.	51
Figure 2.10	TG/DTG trace of oleic acid-coated SPIONs.	52
Figure 2.11	M vs H curve of oleic acid-coated SPIONs.	53
Figure 3.1	Preparation of SPION-Polymeric Micelles– (a) Synthesis of PMMA-Br macroinitiator by ATRP; (b) Chain extension of PMMA-Br with PEGMA to yield PMMA-b-pPEGMA copolymer; (c) Micellization and loading of	60

## SPIONs in polymeric micelles.

- Figure 3.2  $^1\text{H-NMR}$  of PMMA-Br macroinitiators- (a)  $M_1$ , and (b)  $M_2$ . Peaks at 3.6 and 4.12 ppm are due to  $-\text{OCH}_3$  (methacrylate group of repeat unit),  $-\text{OCH}_2\text{CH}_3$  (initiator) respectively. 67
- Figure 3.3 GPC traces depicting elution curves of (a) macroinitiator  $M_1$  and the copolymers  $M_1\text{EG}_1$  and  $M_1\text{EG}_2$  and (b)  $M_2$  and  $M_2\text{EG}_1$ . 68
- Figure 3.4 UV-Vis spectra of  $M_1\text{EG}_1$ ,  $\text{FM}_1\text{EG}_1$  and folic acid (inset). Folic acid shows characteristic absorption at  $\lambda_{\text{max}}=363$  nm. 69
- Figure 3.5 Determination of critical micellar concentration- (a) Pyrene emission spectra for  $M_1\text{EG}_1$  at concentrations 0.01 mg/L and 15 mg/L,  $\lambda_{\text{ex}}=349$  nm; (b-e)  $I_{383}/I_{373}$  is plotted as a function of concentration for various polymers: (b)  $M_1\text{EG}_1$ , (c)  $M_1\text{EG}_2$ , (d)  $M_2\text{EG}_1$  and (e)  $\text{FM}_1\text{EG}_1$ . 71
- Figure 3.6 TEM micrographs of (a)  $M_1\text{EG}_1$ ; (b) a single micelle, core-shell morphology is visible; (c)  $\text{FM}_1\text{EG}_1$  and (d) AFM image of  $\text{FM}_1\text{EG}_1$ . 72
- Figure 3.7 TEM micrograph-  $\text{SPIO}_1(\text{L})$ -Polymer micelle cluster. 73
- Figure 3.8 Magnetic resonance imaging of micellar-SPION clusters ( $\text{FM}_1\text{EG}_1$ - $\text{SPIO}_1(\text{L})$ )– (a) T2-weighted images of the clusters in phantom agar gels; (b) T2 relaxation analysis curves at different concentration of Fe; (c) T2 relaxation rate ( $1/T_2$ ) as a function of Fe concentration (mM). 75
- Figure 3.9 Cytotoxicity evaluation of SPION-loaded micelles. HeLa cells were incubated with (a) 20  $\mu\text{g/ml}$  Fe, and (b) 50  $\mu\text{g/ml}$  Fe of folate conjugated ( $\text{FM}_1\text{EG}_1$ ) and unconjugated ( $M_1\text{EG}_1$ ) micelle- $\text{SPIO}_1(\text{L})$  clusters for 1, 6, 24 h and their viability was evaluated against untreated control cells by MTT assay. (c) Dose response of  $\text{FM}_1\text{EG}_1$ - and  $M_1\text{EG}_1$ -  $\text{SPIO}_1(\text{L})$  clusters on % cell viability of HeLa cells at 24 h treatment duration. Error bars indicate mean  $\pm$  SD (n=3). 77
- Figure 3.10 Intracellular localization of  $\text{FM}_1\text{EG}_1$ - and  $M_1\text{EG}_1$ -  $\text{SPIO}_1(\text{L})$  clusters in HeLa cells when external medium is folate deficient (a) or when it contained folic acid (b). (c) Comparison of internalization of folate-conjugated SPION clusters ( $\text{FM}_1\text{EG}_1$ - $\text{SPIO}_1(\text{L})$ ) with and without receptor-blocking (folate-containing vs. folate-deficient medium). Error bars indicate mean  $\pm$  SD (n=3). 78
- Figure 3.11 Confocal microscopy – (a-c)  $\text{FM}_1\text{EG}_1$ - $\text{SPIO}_1(\text{L})$  clusters incubated with HeLa cells for 24 h, folate-deficient medium; (d-f)  $M_1\text{EG}_1$ - $\text{SPIO}_1(\text{L})$ , 24 h incubation, folate-deficient medium; (g-i)  $\text{FM}_1\text{EG}_1$ - $\text{SPIO}_1(\text{L})$ , 24 h incubation, folate-supplemented medium; (j-l)  $\text{FM}_1\text{EG}_1$ - $\text{SPIO}_1(\text{L})$ , 6 h incubation, folate-deficient medium; (m-o)  $\text{FM}_1\text{EG}_1$ - $\text{SPIO}_1(\text{L})$  cluster, 1 h incubation, folate-deficient medium. 80

Figure 4.1	Schematic representation- SPIONs [SPION <sub>1</sub> (L)] encapsulated in gelatin nanoparticles by desolvation of a gelatin/SPION dispersion.	87
Figure 4.2	Schematic representation of synthesis of mannosylated MGNP.	88
Figure 4.3	Dynamic Light Scattering- Particle size and size distribution of the sample prepared at pH 3 using gelatin concentration of 10 mg/ml and glutaraldehyde concentration of 200 µg/mg gelatin.	94
Figure 4.4	(a) TEM and (b) AFM micrographs of GNP.	96
Figure 4.5	Particle stability on storage for 30 days- (a) TEM (b) Average diameter by DLS.	96
Figure 4.6	TEM micrographs of (a) MGNP and (b) MN-MGNP.	97
Figure 4.7	FT-IR spectra- (a) MN-MGNP and (b) MGNP.	98
Figure 4.8	Colloidal stability of SPION-loaded gelatin nanoparticles- The agglomeration behavior of (a) MGNP and (b) MN-MGNP in different media.	100
Figure 4.9	Stability of MGNP and MN-MGNP in PBS- Measurement of hydrodynamic diameter.	101
Figure 4.10	Magnetic resonance imaging- (a) T2-weighted images of MGNP and MN-MGNP; (b) T2 relaxation rate (1/T2) plotted as a function of Fe concentration (mM).	102
Figure 4.11	Cytotoxicity evaluation of SPION-loaded micelles. HeLa cells were incubated with (a) 20 µg/ml Fe, and (b) 50 µg/ml Fe of MGNP and MN-MGNP for 1, 6, 24 h and their viability was evaluated against untreated control cells by MTT assay. (c) Dose response of MGNP and MN-MGNP on % cell viability of J774 cells at 24 h treatment duration. Error bars indicate mean ± SD (n=3).	103
Figure 4.12	(a) Calibration curve- Colorimetric assay by Prussian blue quantification; Intracellular localization of MGNP and MN-MGNP in J774e cells when external medium is mannose-free (a); or when it contained mannose (b). (c) Comparison of internalization of mannose-conjugated gelatin-SPION nanoparticles with and without receptor-blocking (mannose-containing vs. mannose-deficient medium). Error bars indicate mean ± SD (n=3).	104
Figure 4.13	Cellular internalization- MN-MGNP incubated with J774e murine macrophages for (a) 1h, (b) 6 h and (c) 24 h. (d) MGNP incubated with cells for 24 h. Cells containing internalized iron oxide nanoparticles stain blue, with the intensity of colour dependent upon the extent of internalization.	106
Figure 5.1	Schematic representation of polymer syntheses- Copolymerization	113

	yielding (a) copolymer PEGME-MA/TMSPMA (CP1) and (b) tercopolymers of PEGME-MA/TMSPMA/TMSMA (CP2 and CP3).	
Figure 5.2	Schematic representation of ligand exchange on SPION surface– Replacement of oleic acid with PEG-silanes.	115
Figure 5.3	TEM micrographs of SPIONs dispersed in PBS– (a) MNP-Si-PEG; (b) MNP-Si-CPEG2 and (c) MNP-PEI2.	123
Figure 5.4	Particle size distribution and correlation curve from DLS measurement of sample MNP-Si-PEG, in PBS (pH 7.4).	124
Figure 5.5	FT-IR spectra– (a) oleic acid-coated SPIONs; (b) MNP-Si-PEG; (b) MNP-Si-CPEG1 and (c) MNP-Si-CPEG2.	126
Figure 5.6	FT-IR spectra– (a) MNP-Si-CPEG2; (b) PEI; (c) MNP-PEI1 and (d) MNP-PEI2.	127
Figure 5.7	TG/DTG traces of coated SPIONs and copolymers– (a) MNP-Si-PEG; (b) MNP-Si-CPEG1; (c) MNP-Si-CPEG2; (d) MNP-PEI1; (e) MNP-PEI2; (f) copolymer CP1; (g) copolymer CP2; and (h) copolymer CP3.	130
Figure 5.8	Turbidimetry studies for colloidal stability of coated SPIONs– (a) MNP-Si-PEG; (b) MNP-Si-CPEG1; (c) MNP-Si-CPEG2; (d) MNP-PEI1; and (e) MNP-PEI2.	132
Figure 5.9	Magnetic resonance imaging of MNP-Si-PEG – (a) T2-weighted images of the SPIONs in phantom agar gels; (b) T2 relaxation analysis curves at different concentration.	133
Figure 5.10	Cytotoxicity– HeLa cells are incubated with polymer coated SPIONs (20 µg/ml) for 1, 6 and 24 h. Error bars indicate mean ± SD (n=3).	134
Figure 5.11	(a) Calibration curve– Colorimetric assay by Prussian blue quantification; (b) Uptake of polymer-modified SPIONs in HeLa cells incubated with particles at a concentration of 20 µg/ml (Fe) for 1, 6 and 24 h. Error bars indicate mean ± SD (n=3).	135
Figure 6.1	Carbodiimide coupling between –COOH of folic acid and -OH groups PEG chains of copolymer.	143
Figure 6.2	Mannosylation of SPION-loaded gelatin nanoparticles (MGNP).	146

## LIST OF TABLES

Table no.	Table title	Page no.
Table 1.1	List of iron oxide based contrast agents that are commercialized or in various stages of clinical trials	18
Table 2.1	d-spacing for sample SPIO(L) <sub>1</sub> calculated from peak positions in XRD pattern and compared with standard JCPDS values for magnetite; corresponding hkl indices	43
Table 3.1	Polymer composition, molecular weight and polydispersity	66
Table 4.1	Effect of gelatin concentration on nanoparticle size and particle size distribution. Glutaraldehyde concentration is 200 µg/mg gelatin, pH=3	94
Table 4.2	Effect of medium pH and glutaraldehyde concentration on GNP size and zeta potential. Gelatin concentration is 10 mg/ml.	95
Table 5.1	Feed compositions used in synthesis of copolymers CP1, CP2 and CP3.	113
Table 5.2	Copolymer characterization by GPC and FT-IR.	122
Table 5.3	Hydrodynamic diameter and zeta potential of modified SPIONs, measured in PBS (pH 7.4).	124
Table 6.1	Polymer compositions- Feed ratios of monomer, initiator and catalyst.	142
Table 6.2	Comparison of important properties of differently modified SPIONs	151



## ABBREVIATIONS

AFM	Atomic force microscopy
ANOVA	Analysis of variance
ATRP	Atom transfer radical polymerization
BPO	Benzoyl peroxide
CMC	Critical micellar concentration
DCC	N,N'-Dicyclohexylcarbodiimide
DLS	Dynamic light scattering
DMAP	4-Dimethylaminopyridine
DMdP	4,4'-Dimethyl-2,2'-dipyridyl
DMEM	Dulbecco's modified Eagle's medium
DMF	Dimethylformamide
DMSO	Dimethylsulphoxide
EAT	Ehrlich Ascites tumor
EBiB	Ethyl $\alpha$ -bromoisobutyrate
EDAC	N-(3-Dimethylaminopropyl)-N'-ethylcarbodiimide hydrochloride
FA	Folic acid
FBS	Fetal bovine serum
FCS	Fetal calf serum
FDA	Food and Drug Administration (USA)
FR- $\alpha$	Folate receptor- $\alpha$ isoform
FT-IR	Fourier transform - Infrared spectroscopy
GNP	Gelatin nanoparticles
GPC	Gel permeation chromatography
HRTEM	High resolution transmission electron microscopy
MGNP	Magnetic gelatin nanoparticles
MMA	Methyl methacrylate
MN-MGNP	Mannosylated magnetic gelatin nanoparticles
MRI	Magnetic resonance imaging

MTT	3-(4,5-Dimethylthiazol-2-yl)-2,5-diphenyltetrazolium bromide
NHS	N-Hydroxysuccinimide
NMR	Nuclear magnetic resonance
OA	Oleic acid
PBS	Phosphate buffered saline
PDI	Polydispersity index
PEG	Poly(ethylene glycol)
PEGMA	Poly(ethylene glycol) methacrylate
PEGME-MA	Poly(ethylene glycol) methyl ether methacrylate
PEI	Poly(ethyleneimine)
RES	Reticuloendothelial system
RPMI	Roswell Park Memorial Institute medium
SAED	Selected area electron diffraction
SPIO	Superparamagnetic iron oxide
SPION	Superparamagnetic iron oxide nanoparticles
TEM	Transmission electron microscopy
TGA	Thermogravimetric analysis
THF	Tetrahydrofuran
TMSMA	Trimethylsilyl methacrylate
TMSPMA	3-(Trimethoxysilyl)propyl methacrylate
TREG	Triethylene glycol
VSM	Vibrating scanning magnetometry
XRD	X-ray diffraction